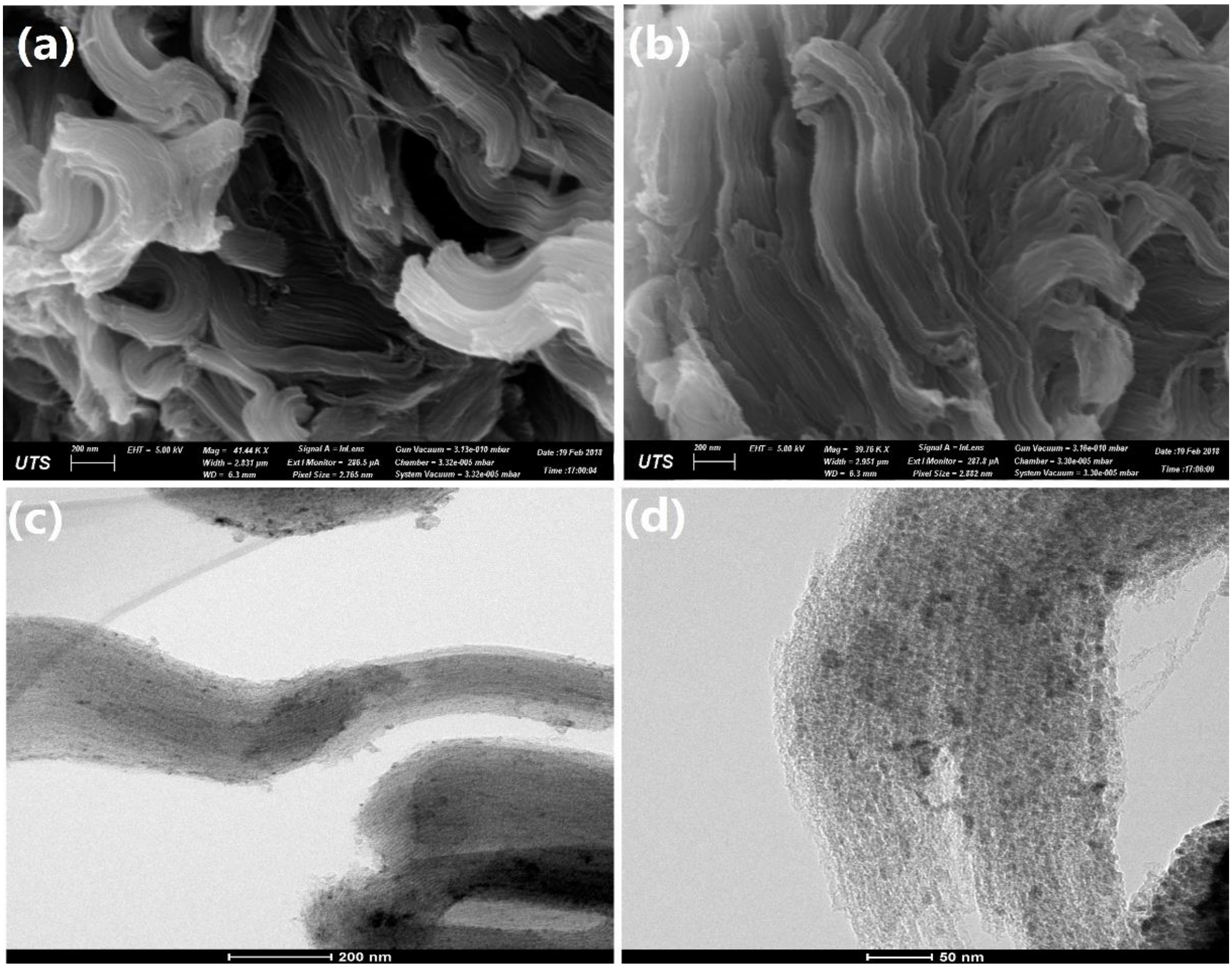

Supplementary Figure 1 | Morphology characterization. SEM images of **(a)** TiO_2-OMC and **(b)** TiN-OMC, TEM images of **(c)** TiO_2-OMC and **(d)** TiN-OMC.

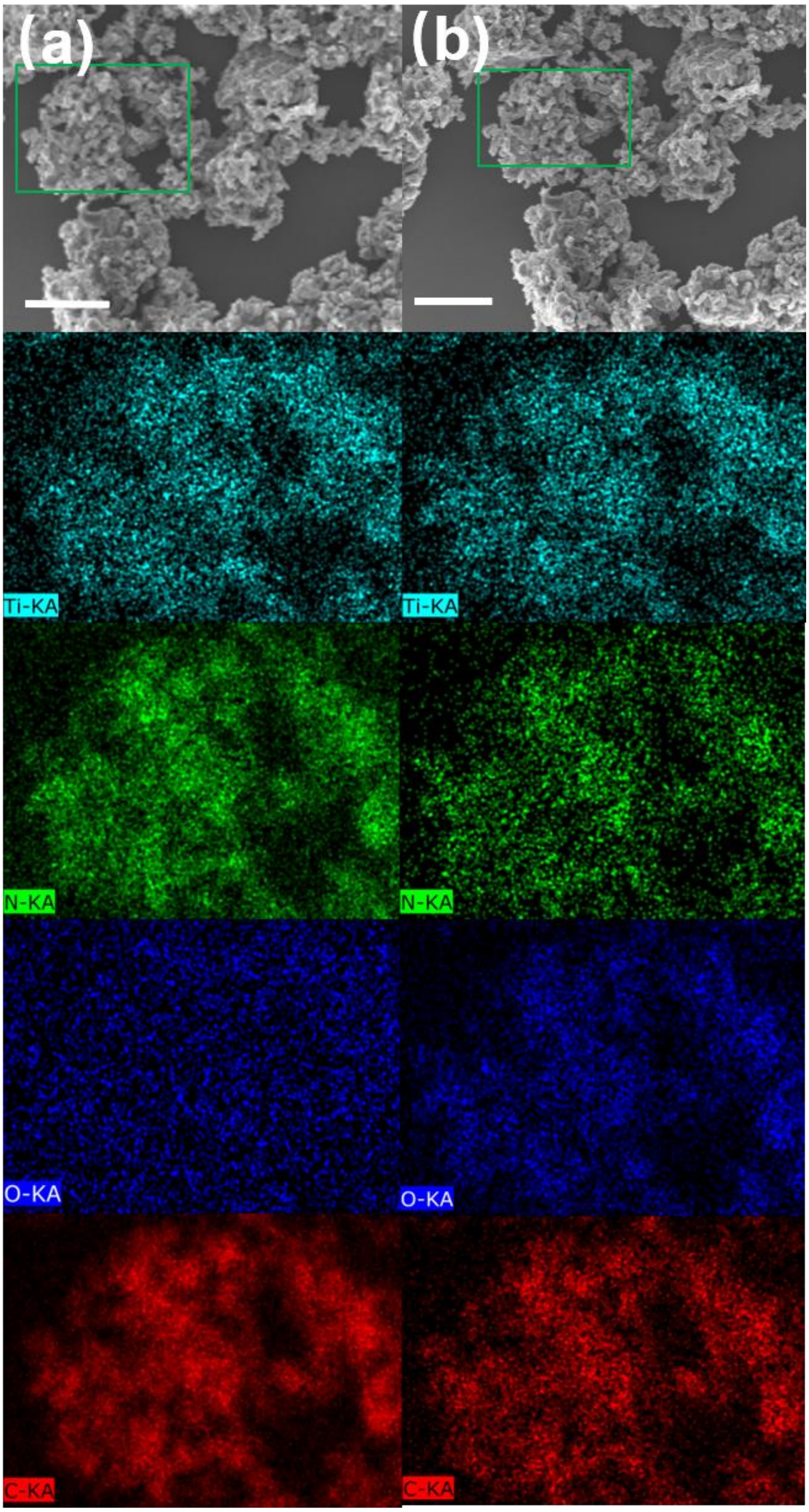

Supplementary Figure 2 | Elemental mapping. SEM elemental mapping images of **(a)** TiN-OMC and **(b)** TiN-O-OMC. Scale bar: (a, b) 2 μm. Green lines: selected area for elemental mapping.

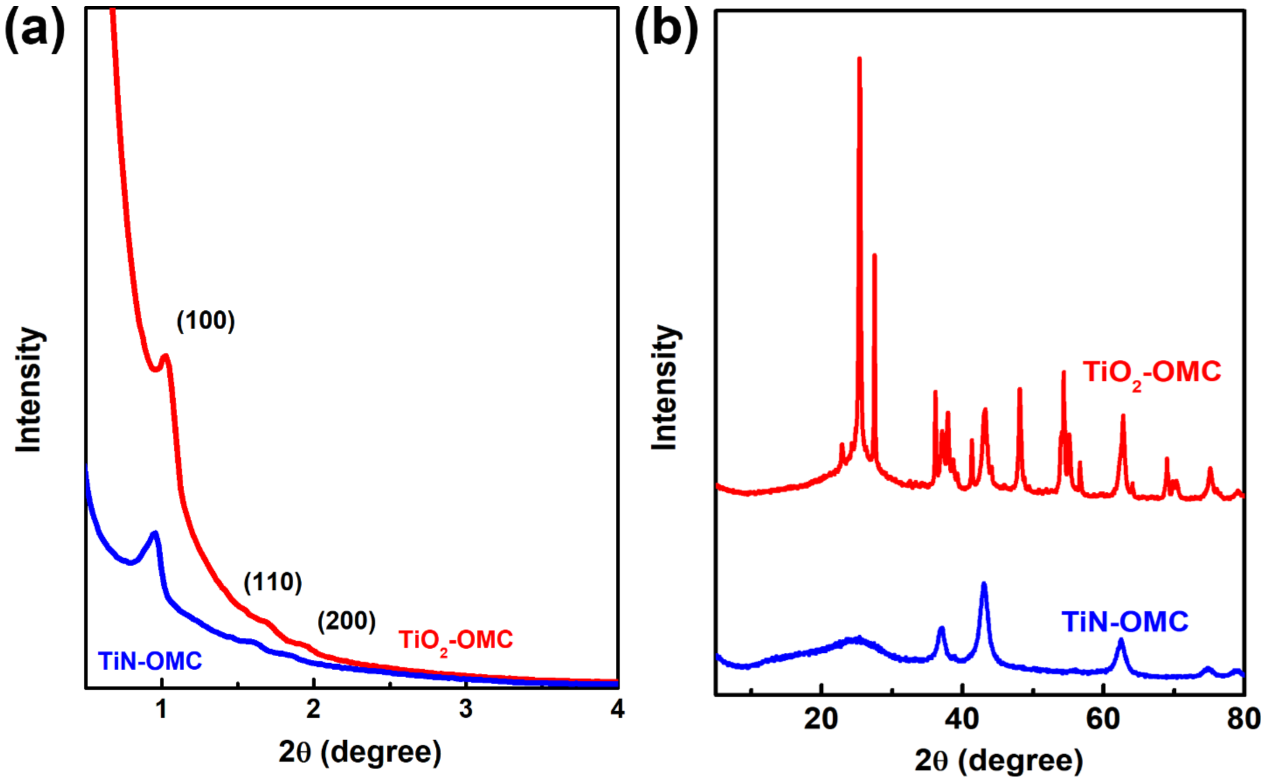

Supplementary Figure 3 | Crystalline analysis. (a) Small-angle and **(b)** wide-angle XRD patterns for TiO_2-OMC and TiN-OMC.

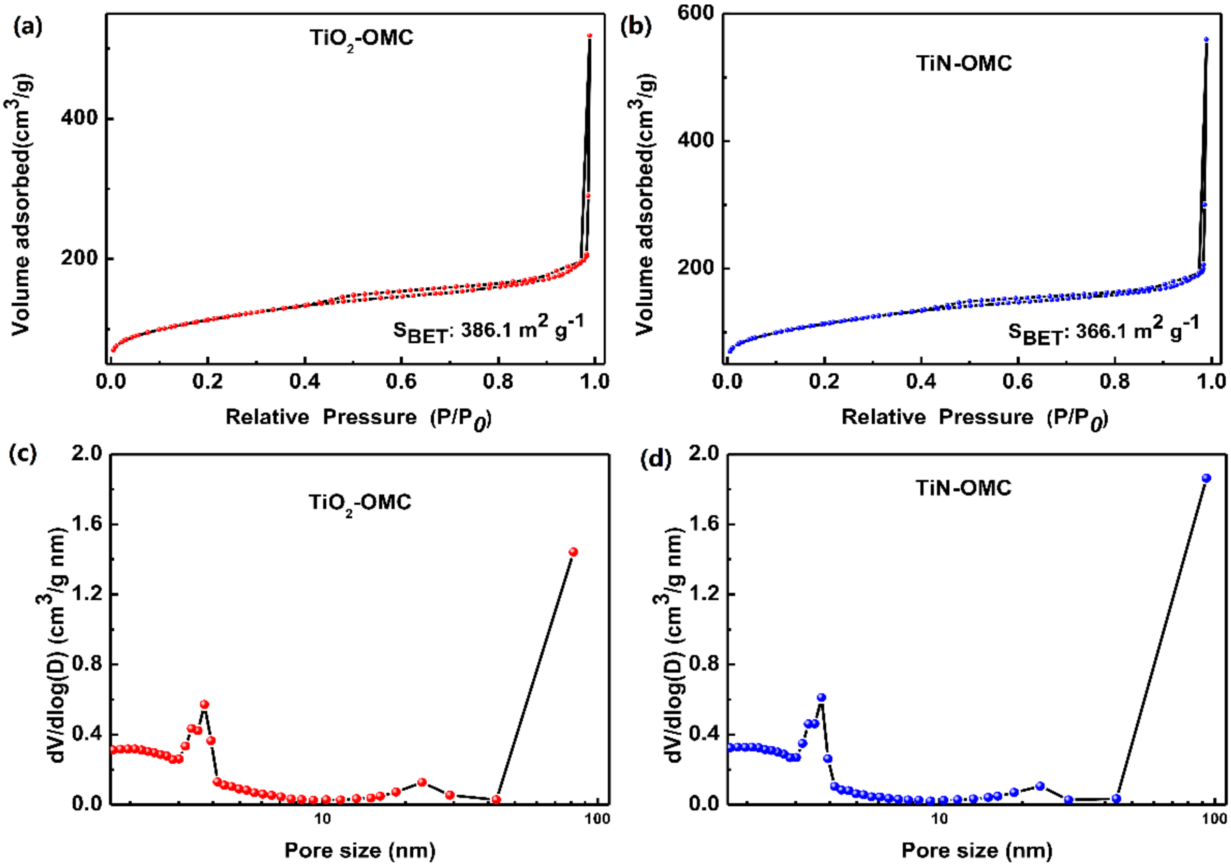

Supplementary Figure 4 | Structure Analysis. N_2 adsorption-desorption isotherms of **(a)** TiO_2-OMC, **(b)** TiN-OMC and the corresponding pore size distribution plots of **(c)** TiO_2-OMC and **(d)** TiN-OMC.

Supplementary Table 1. Comparison of BET surface area, pore volume and pore size distribution of SBA-15, OMC, TiO2-OMC, TiN-OMC and TiN-O-OMC.

Samples	BET surface area (m^2 g^{-1})	Pore volume (cm^3 g^{-1})	Pore size distributions (nm)
SBA-15	587.1	1.38	6.2-7.8
OMC	726.3	0.78	3.1-4.0
TiO_2-OMC	355.9	0.81	3.2-4.1
TiN-OMC	386.1	0.82	3.2-4.2
TiN-O-OMC	355.9	0.88	3.1-4.1

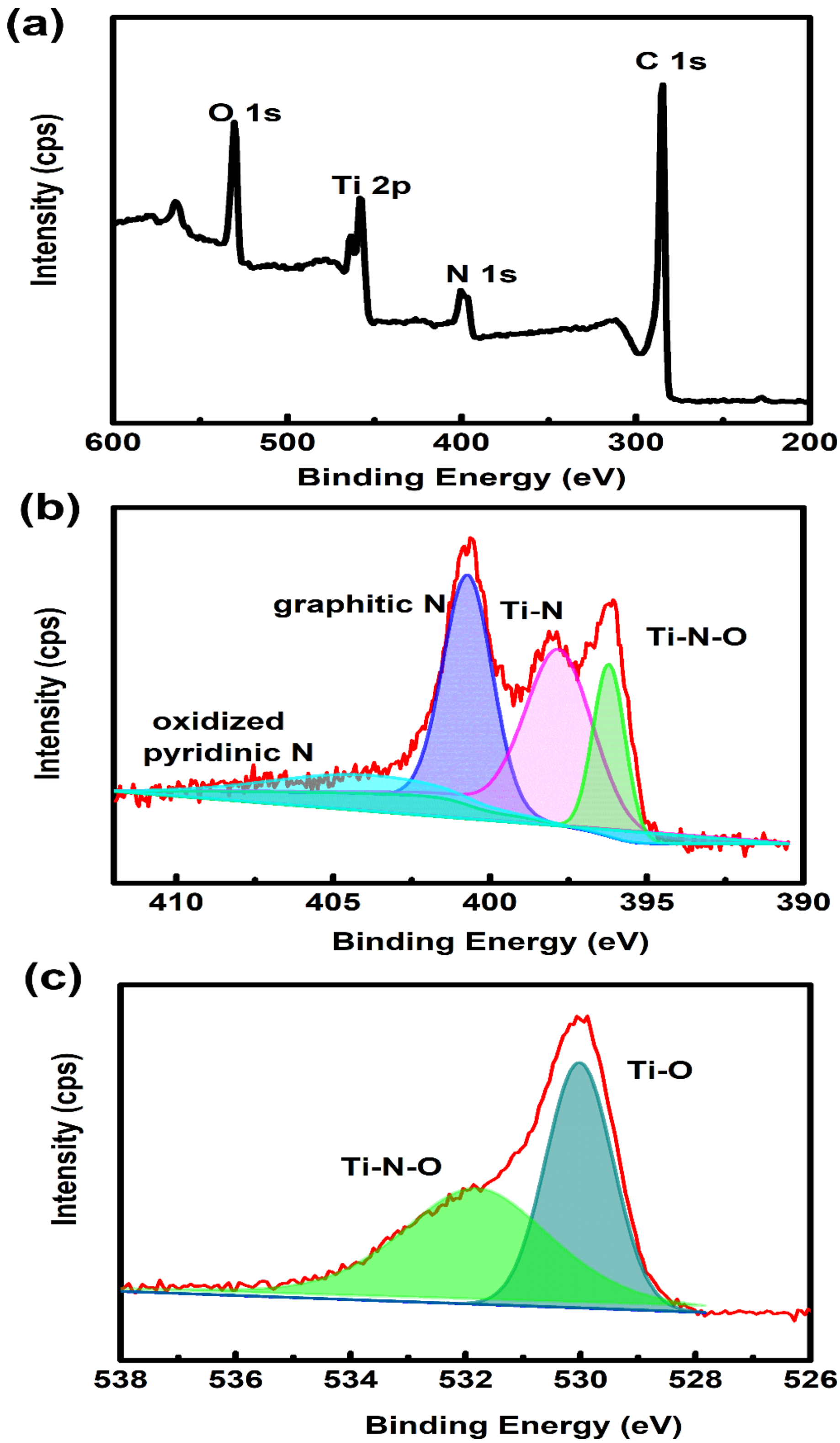

Supplementary Figure 5 | XPS analysis of TiN-O-OMC. (a) The survey XPS spectrum. High-resolution XPS spectrum of **(b)** N 1s and **(c)** C 1s.

Supplementary Table 2. Elements content of TiN-O-OMC.

Elements	Ti*	N*	C	O
Content (at. %)	5.79	9.62	72.78	11.81

*Footnote: The higher N content (9.62%) than Ti (5.79%) can be ascribed to the N-doping of OMC, which is reflected by the graphitic and oxidized pyridinic N around 400.7 and 403.9 eV in N 1s spectrum (Supplementary Figure 4b).

Supplementary Table 3. Fractions of Ti-containing species for TiN-O-OMC.

Peak position (eV)	464.4	463.1	461.1	458.5	457.0	455.7
Ti-containing specie	O-Ti-O (amorphous)	N-Ti-O	Ti-N	O-Ti-O (amorphous)	N-Ti-O	Ti-N
Content (at. %)	8.8	14.2	9.8	20.7	21.6	24.9
Total	$Ti_{40}N_{28}O_{37}$					

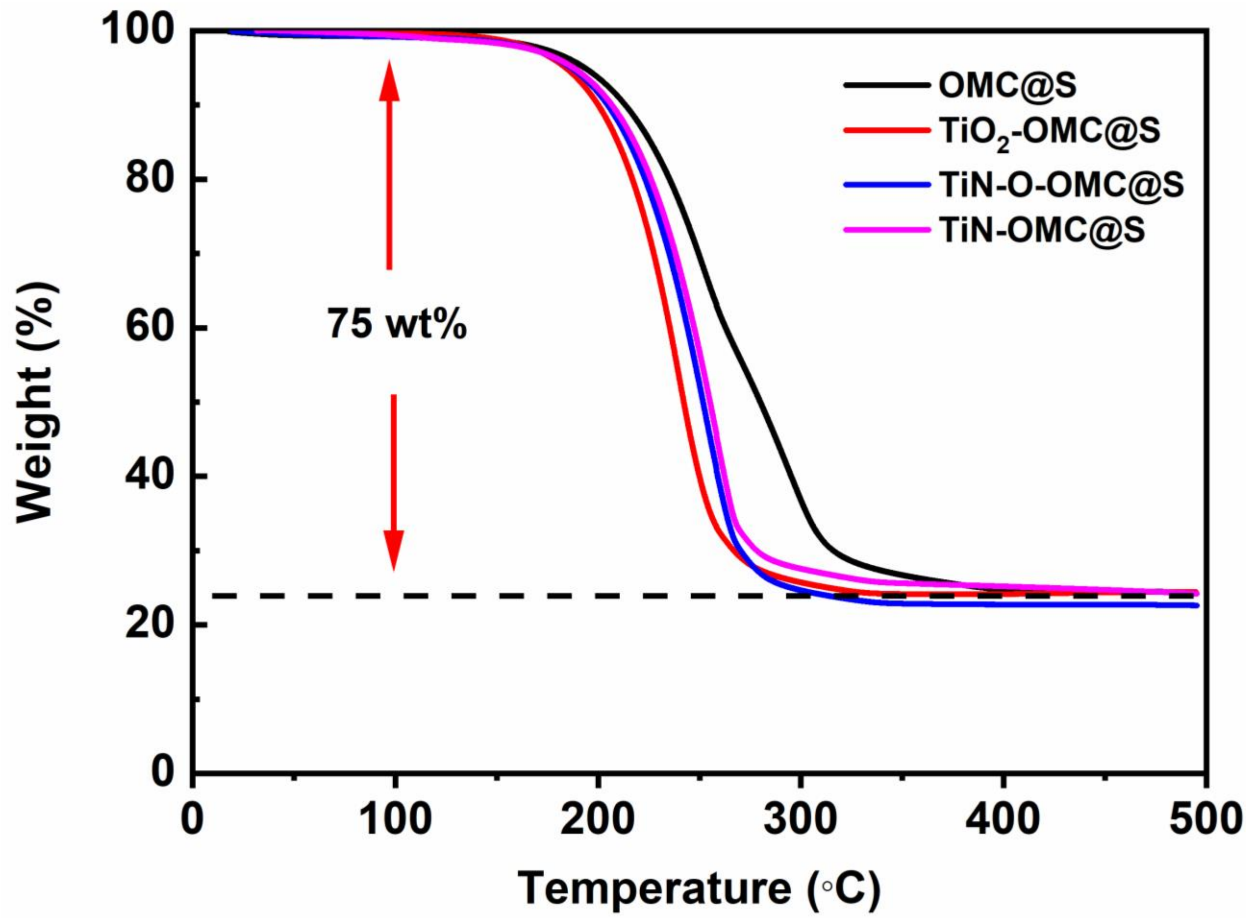

Supplementary Figure 6 | Sulphur compositions. TGA curves of OMC@S, TiO_2-OMC@S, TiN-O-OMC@S and TiN-OMC@S measured under N_2 atmosphere with a heating rate of 10 ºC min^{-1} from room temperature to 500 ºC.

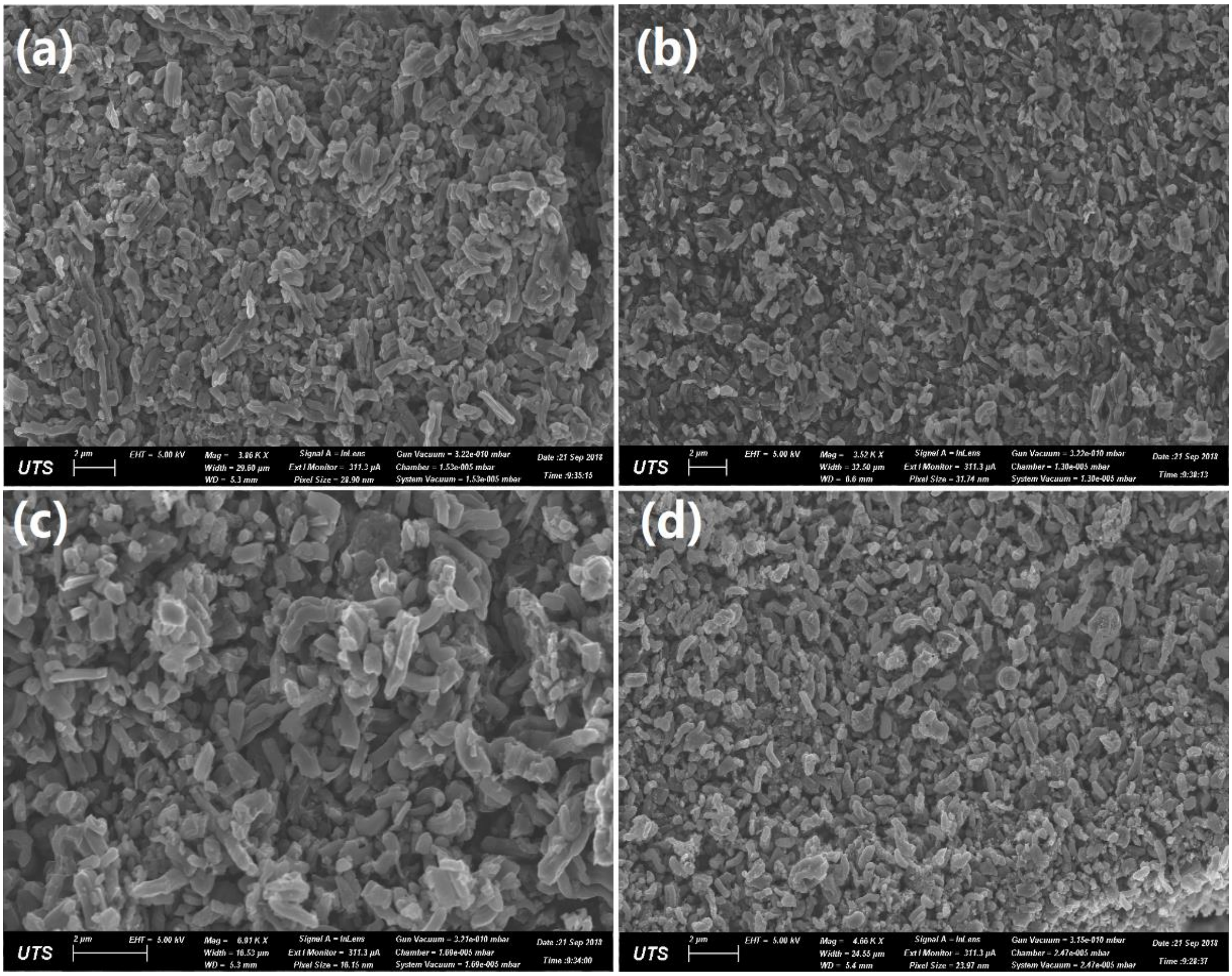

Supplementary Figure 7 | Morphology analysis of S-containing composites. SEM images of **(a)** OMC@S, **(b)** TiN-O-OMC@S, **(c)** TiO_2-OMC@S and **(d)** TiN-OMC@S.

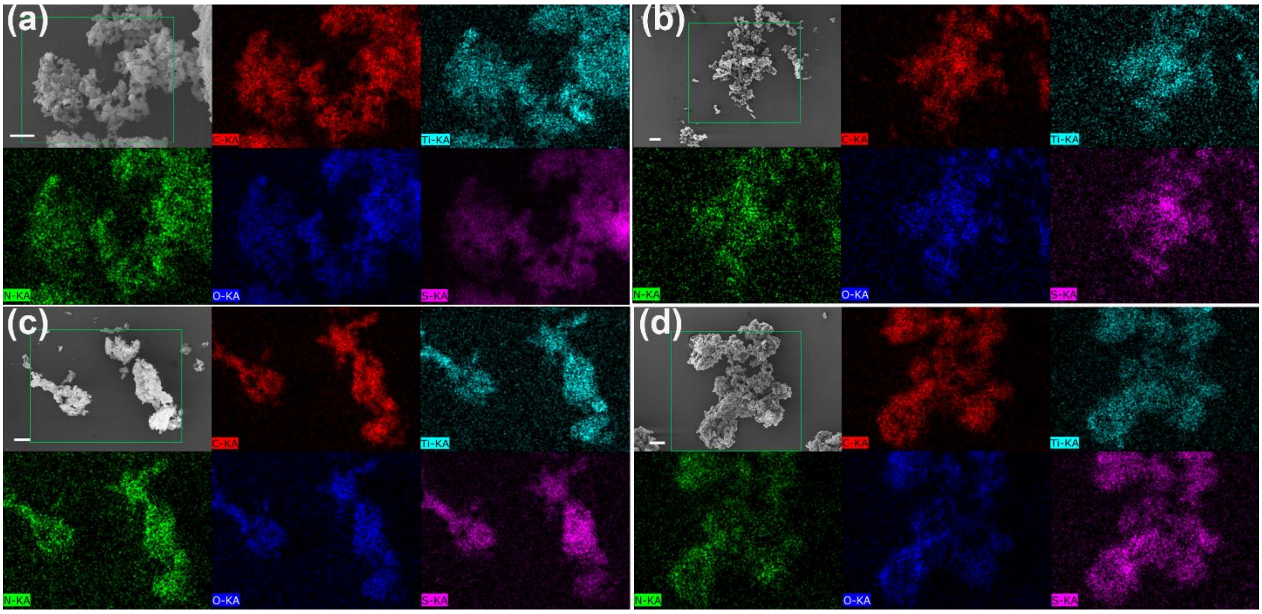

Supplementary Figure 8 | Elemental mapping. SEM elemental mapping images of **(a)** OMC@S, **(b)** TiN-O-OMC@S, **(c)** TiO_2-OMC@S and **(d)** TiN-OMC@S. Scale bar: (a-d) 2 μm. Green lines: selected area for elemental mapping.

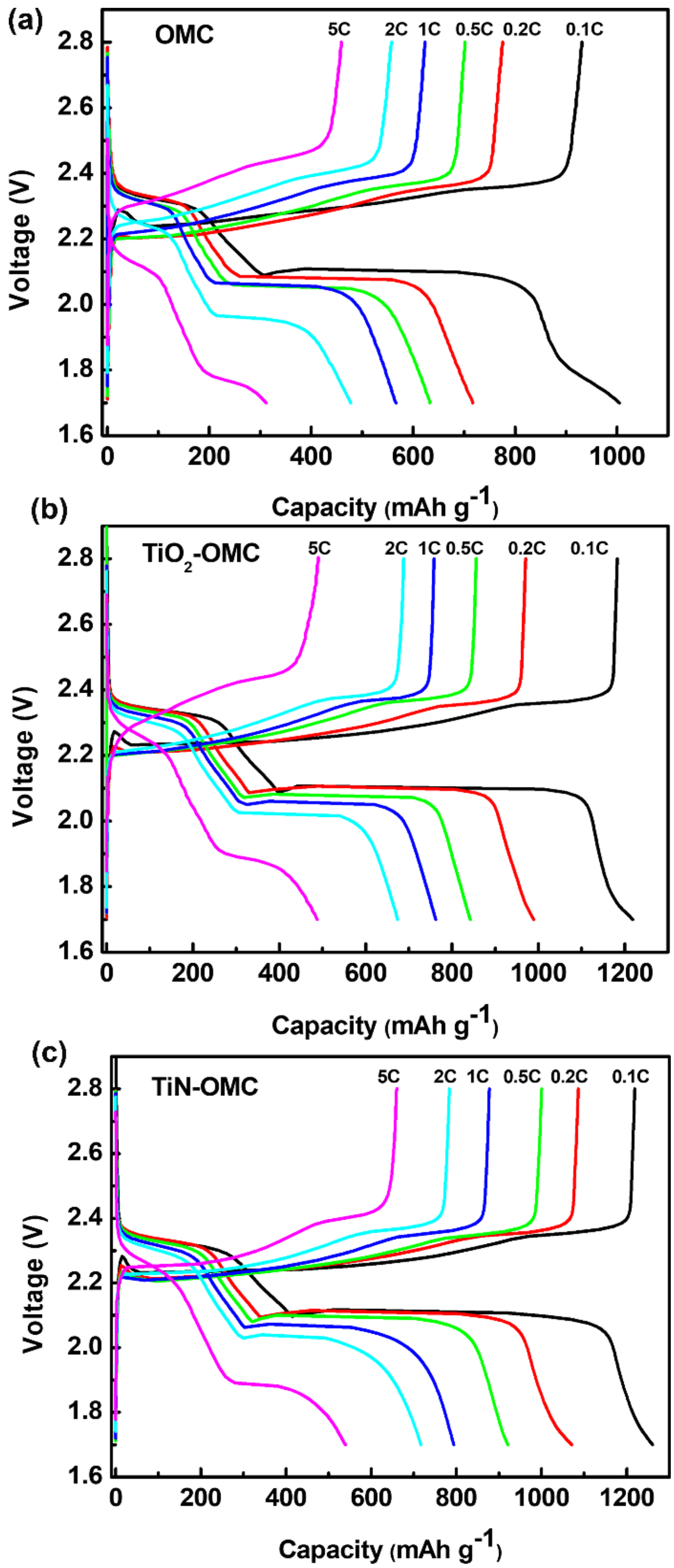

Supplementary Figure 9 | Electrochemical performance. Galvanostatic discharge-charge voltage profiles of **(a)** OMC, **(b)** TiO_2-OMC, and **(c)** TiN-OMC electrodes at various rates from 0.1 to 5 C within the potential window in the range of 1.7 to 2.8 V.

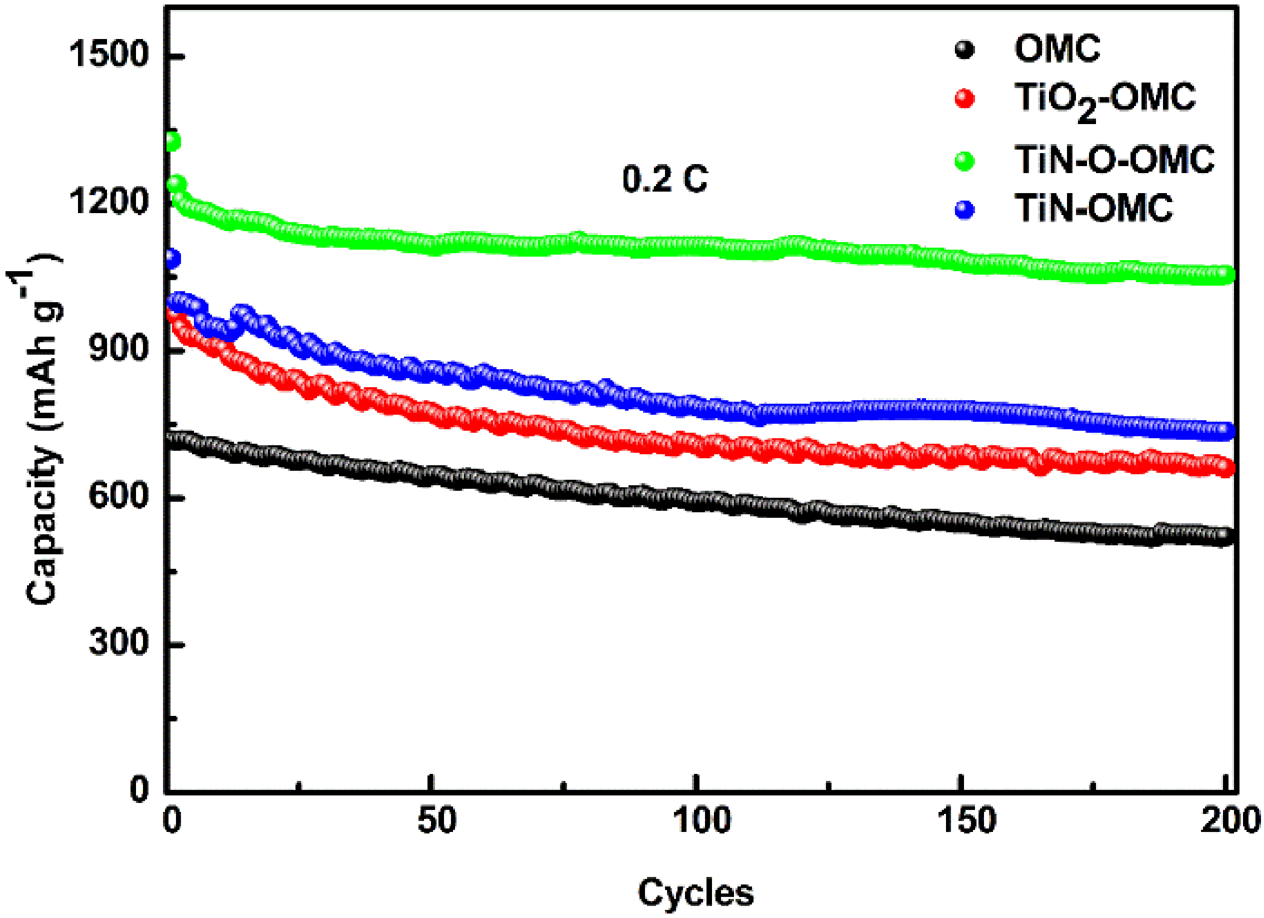

Supplementary Figure 10 | Electrochemical performance. Comparison of cycling stability at 0.2 C of OMC, TiO_2-OMC, TiN-OMC and TiN-O-OMC electrodes within the potential window in the range of 1.7 to 2.8 V.

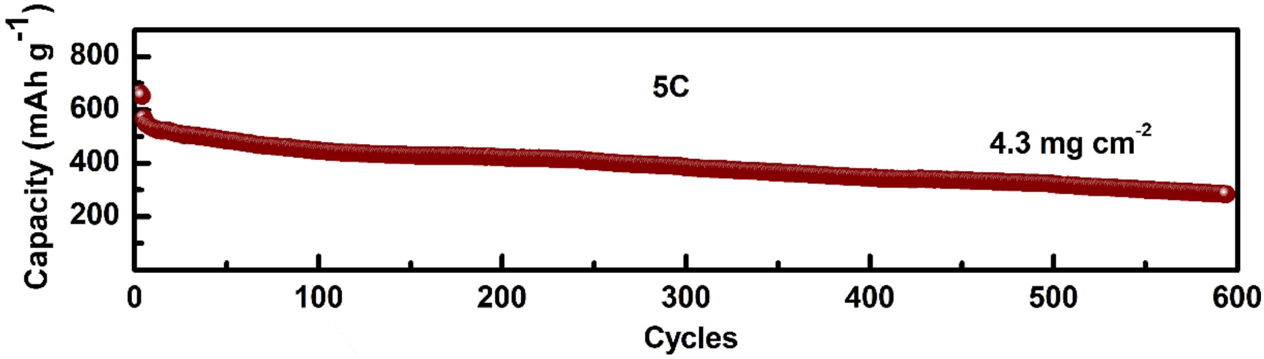

Supplementary Figure 11 | Li-S performance. Cycling stability of TiN-O-OMC@S electrode at 5 C with a high sulphur mass loading of 4.3 mg cm^{-2}.

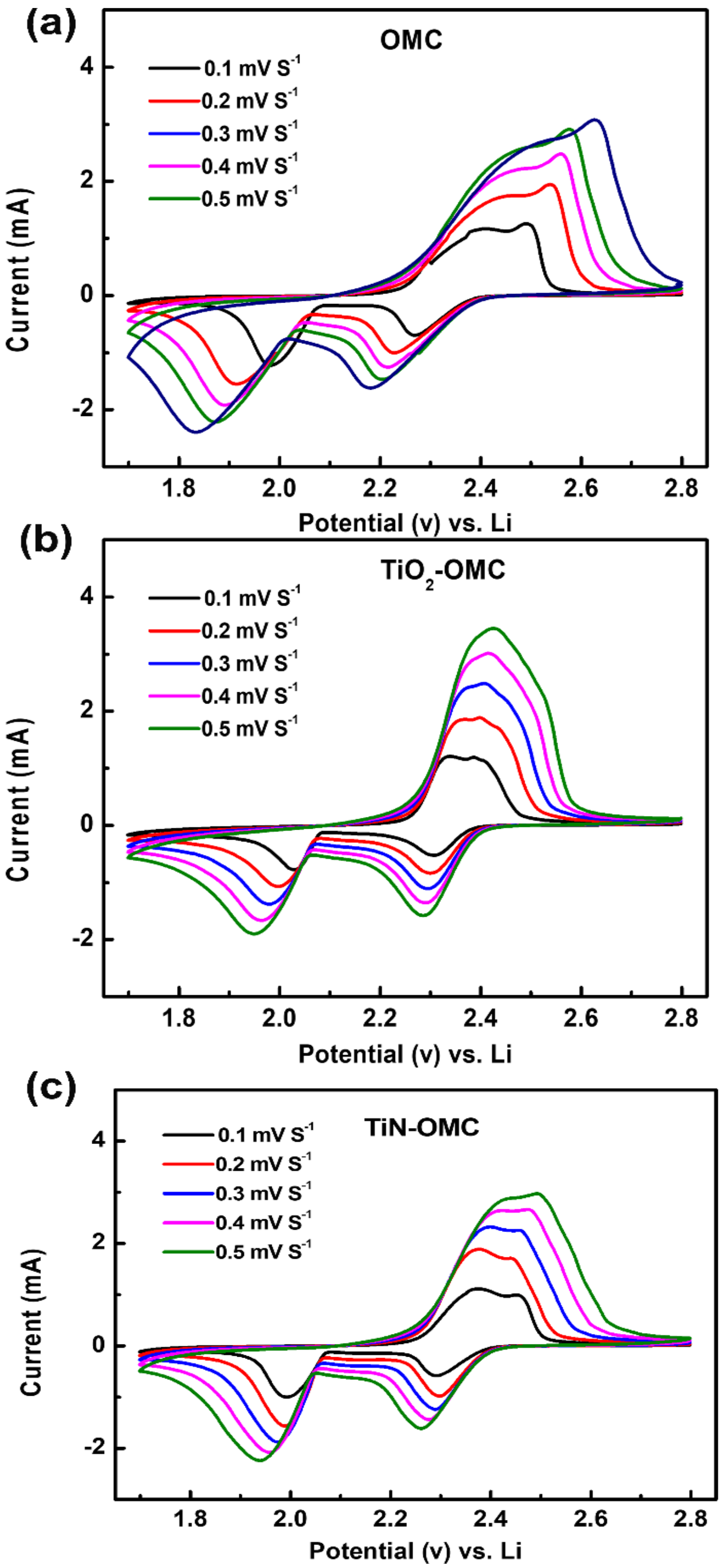

Supplementary Figure 12 |CV scans. CV scans of **(a)** OMC, **(b)** TiO_2-OMC and **(c)** TiN-OMC from 0.1-0.5 mV s^{-1} in a typical Li-S coin cell with Li metal as the counter/reference electrode and commercial Li-S electrolyte.

Supplementary Table 4. Fitting results of EIS of OMC, TiO_2-OMC, TiN-O-OMC and TiN-OMC.

	R_s (Ω)*	**R_{ct} (Ω)***
OMC	3.41	84.82
TiO_2-OMC	4.61	90.85
TiN-OMC	2.33	27.29
TiN-O-OMC	2.23	59.97

*Footnote: The EIS result is fitted employing the equivalent circuit (Insert, R1+ C1/(R2+W1)). The Nyquist plots consist of two parts, one semicircle in the high- and medium frequency (charge transfer resistance, R_{ct}) and an inclined line in the low frequency (diffusion process). The smallest semicircles for the TiN-O-OMC and TiN-OMC electrodes indicate the reduced charge transfer resistance, demonstrating the higher electronic conductivity of TiN than TiO_2 and pure OMC.

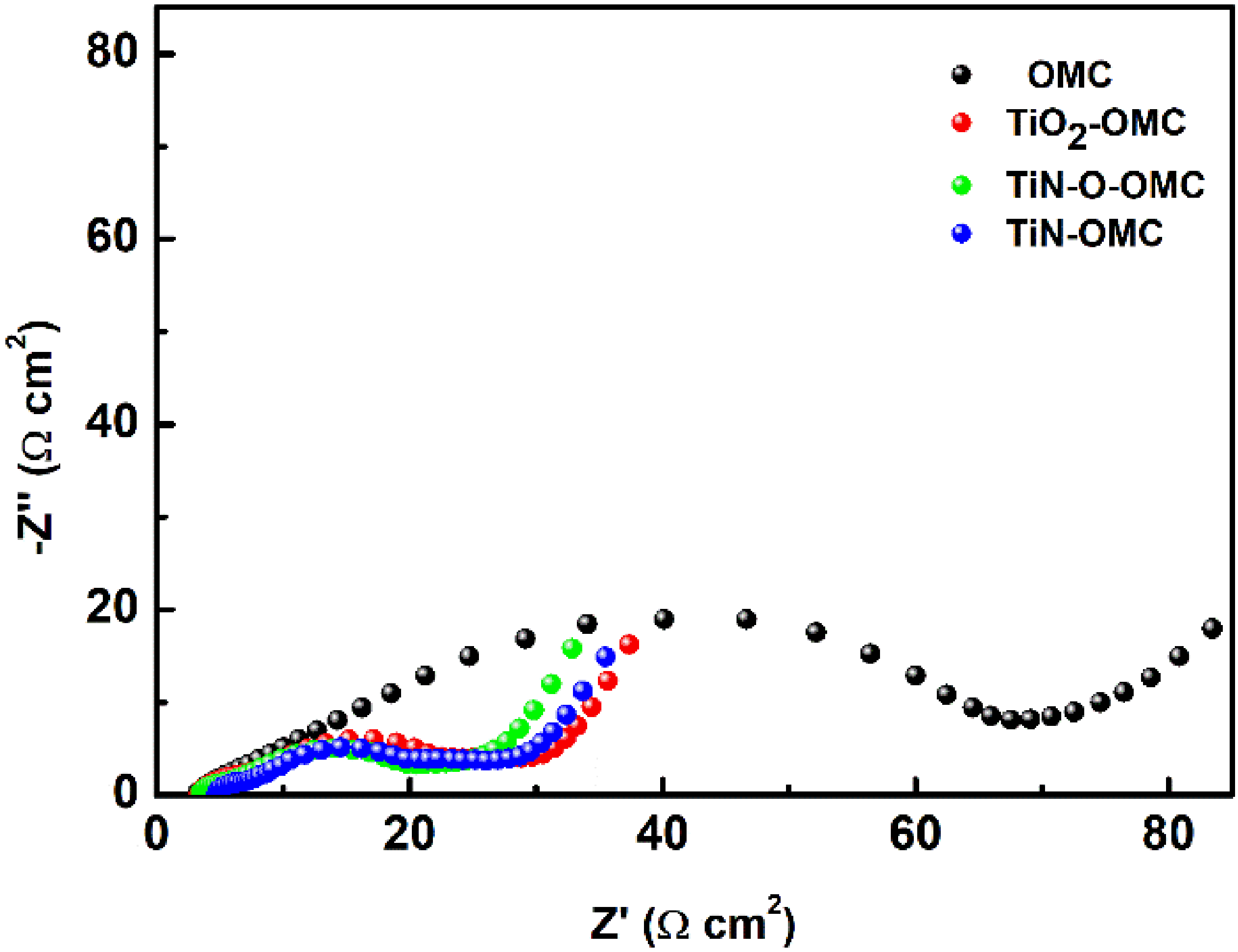

Supplementary Figure 13 | Analysis of Charge transfer resistance. EIS results of symmetric cells containing a 0.4 M Li_2S_6-DOL/DME solution as the electrolyte and OMC, TiO_2-OMC, TiN-OMC and TiN-O-OMC as the electrodes.

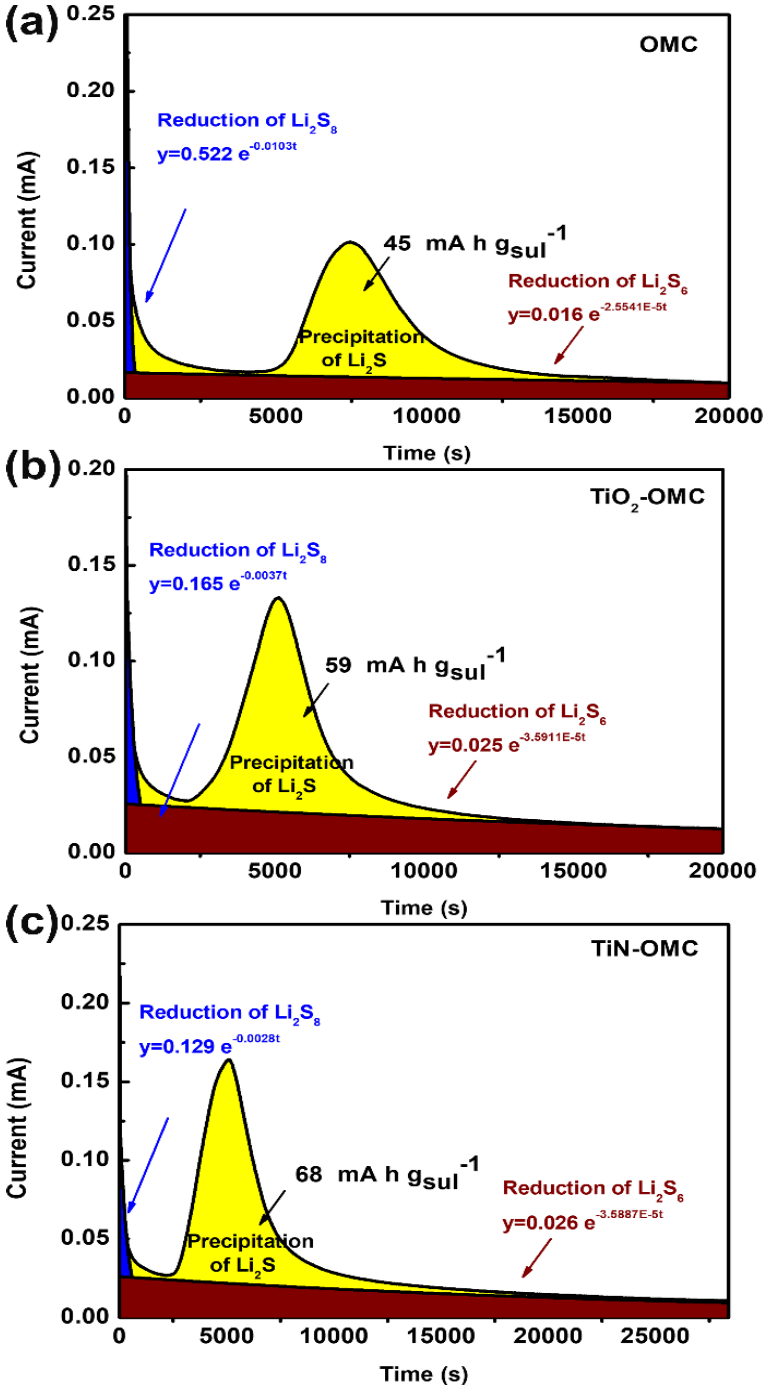

Supplementary Figure 14 | Li_2S precipitation experiment. Fitting of current vs. time curve for potentiostatic discharge at 2.05V of **(a)** OMC, **(b)** TiO_2-OMC and **(c)** TiN- OMC based cathode with Li_2S_8 catholyte.

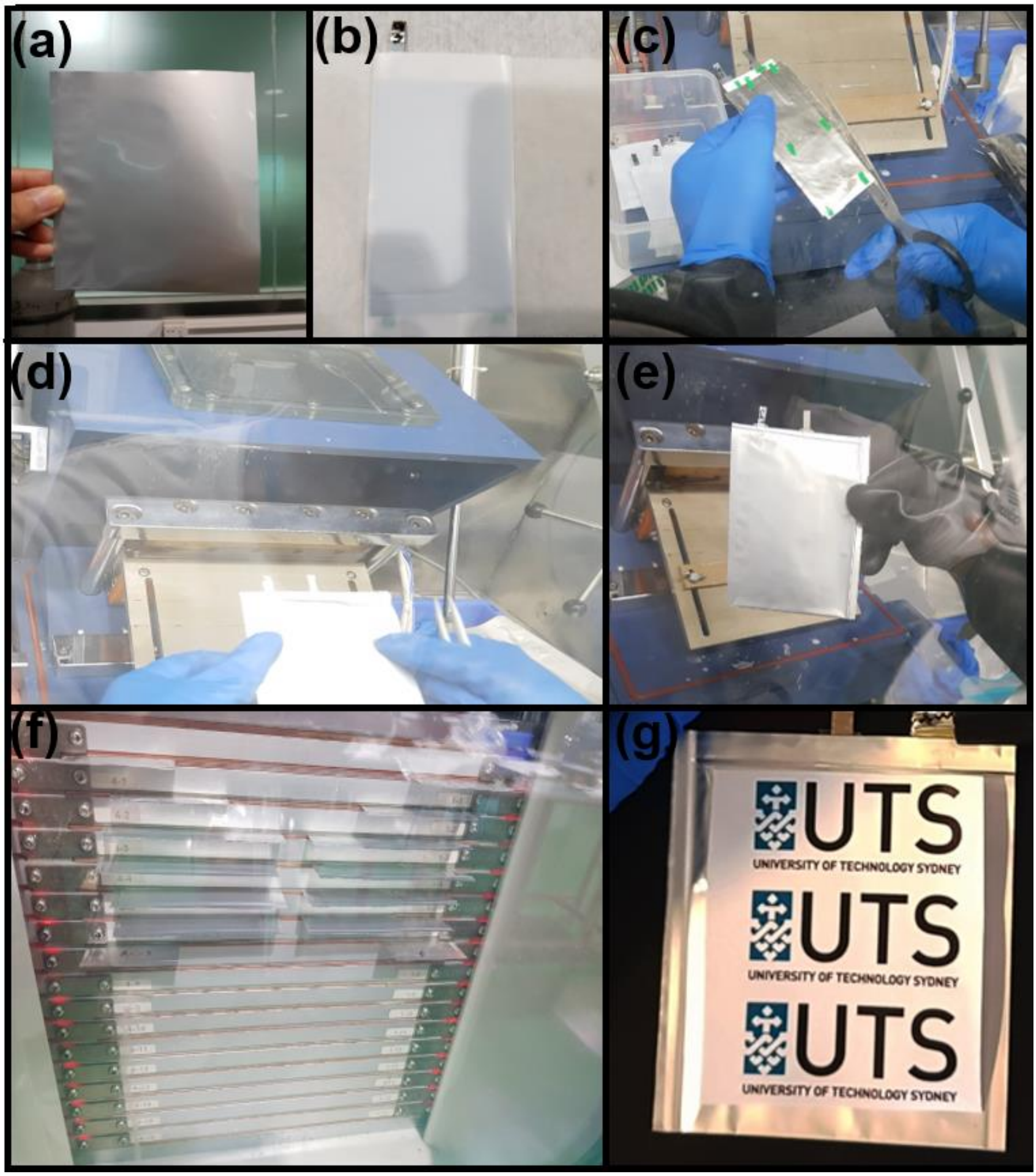

Supplementary Figure 15 | Fabrication of pouch cell. (a) Half-sealed laminate film. **(b)** Separator coated cathode. **(c)** Li foil coated separator along with cathode. **(d)** Side-sealed laminate film. **(e)** Pouch cell after injection of electrolyte and full-sealing. **(f)** Stabilization, cold press and formation of pouch cell. **(g)** Pouch cell ready for testing.

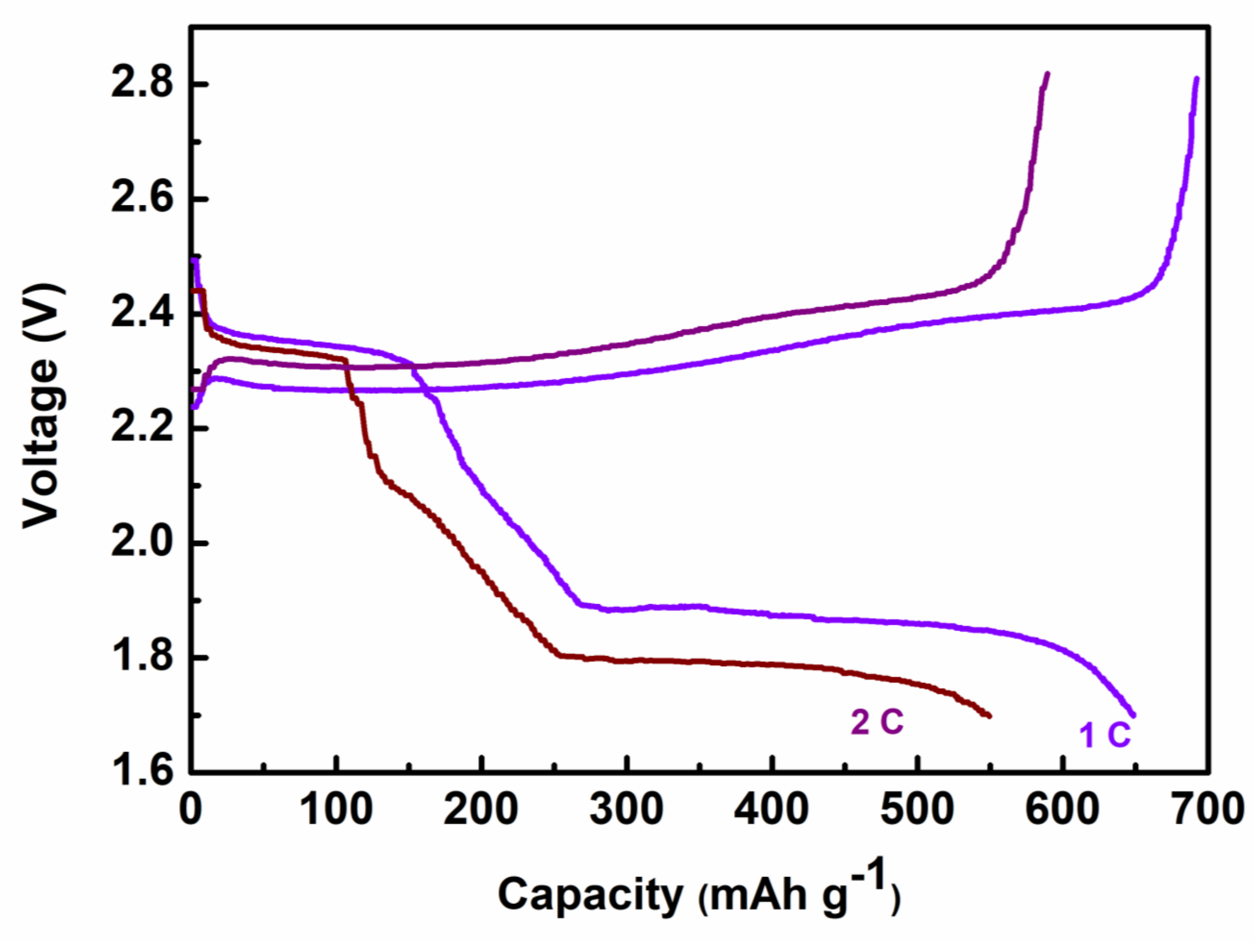

Supplementary Figure 16 | Pouch cell Li-S battery performance at higher rates. Galvanostatic charge/discharge profiles at 1, 2 C of TiN-O-OMC cathodes.

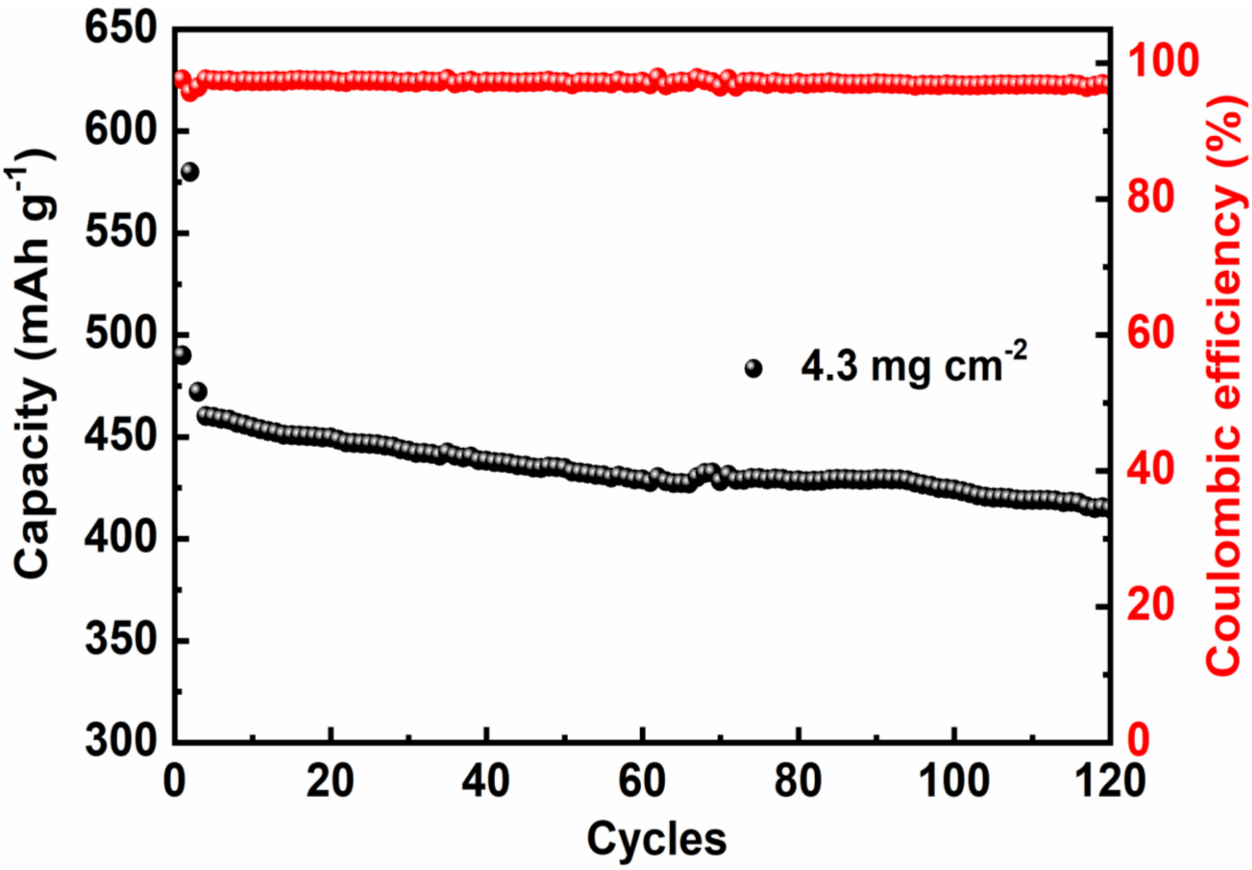

Supplementary Figure 17 | Cycling stability of pouch cell. Cycling performance and Coulombic efficiency at 0.2 C with a sulphur loading of 4.3 mg cm^{-2}.